Обзор ArXiv/astro-ph, 3-7 февраля 2020

От Сильченко О.К.

ArXiv: 2002.01941

The formation of exponential disk galaxies in MOND

Nils Wittenburg,[1] Pavel Kroupa,[1,2] and Benoit Famaey[3]

[1] *University of Bonn, Helmholtz-Institut für Strahlen- und Kernphysik, Nussallee 14-16, D-53115 Bonn, Germany*

[2] *Charles University in Prague, Faculty of Mathematics and Physics, Astronomical Institute, V Holešovičkách 2, CZ-180 00 Praha 8, Czech Republic*

[3] *Université de Strasbourg, Observatoire Astronomique de Strasbourg, CNRS UMR 7550, 11 rue de l'Université, F-67000 Strasbourg, France*

(Accepted in ApJ 18.01.2020)

ABSTRACT

The formation and evolution of galaxies is highly dependent on the dynamics of stars and gas, which is governed by the underlying law of gravity. To investigate how the formation and evolution of galaxies takes place in Milgromian gravity (MOND), we present full hydrodynamical simulations with the Phantom of Ramses (POR) code. These are the first-ever galaxy formation simulations done in MOND with detailed hydrodynamics, including star formation, stellar feedback, radiative transfer and supernovae. These models start from simplified initial conditions, in the form of isolated, rotating gas spheres in the early Universe. These collapse and form late-type galaxies obeying several scaling relations, which was not a priori expected. The formed galaxies have a compact bulge and a disk with exponentially decreasing surface mass density profiles and scale lengths consistent with observed galaxies, and vertical stellar mass distributions with distinct exponential profiles (thin and thick disk). This work thus shows for the first time that disk galaxies with exponential profiles in both gas and stars are a generic outcome of collapsing gas clouds in MOND. These models have a slight lack of stellar angular momentum because of their somewhat compact stellar bulge, which is connected to the simple initial conditions and the negligible later gas accretion. We also analyse how the addition of more complex baryonic physics changes the main resulting properties of the models and find this to be negligibly so in the Milgromian framework.

MOND+RAMSES

lengths and time by a factor λ. Thus, if the actual acceleration g (which scales as λ^{-1}) is a function of the Newtonian gravitational acceleration, $g_{\rm N}$ (which scales as λ^{-2}), their relation has to be of the form shown in Eq. 1. As SI only leads to proportionality in Eq. 1, a_0 needs to be normalized such that equality holds (Milgrom 1983; Milgrom 2009; Wu & Kroupa 2015). Thus, when scale-invariance applies the true gravitational acceleration, g, is given by

$$g = \sqrt{a_0 g_{\rm N}}, \tag{1}$$

where $a_0 \approx 10^{-10}{\rm ms}^{-2} \approx 3.7{\rm pcMyr}^{-2}$ is Milgrom's constant and $g_{\rm N}$ is the Newtonian acceleration.

Eq.1 is the basic equation underlying the MOND paradigm and it is only valid in the low acceleration deep-MOND limit $g \ll a_0 \approx 10^{-10}{\rm ms}^{-2}$. To also encapsulate the symmetry breaking in the Newtonian regime, Milgrom's law is formulated as follows:

$$\mathbf{g} = \nu\left(\frac{g_{\rm N}}{a_0}\right)\mathbf{g}_{\rm N}, \tag{2}$$

with $\nu(y)$, $y = g_{\rm N}/a_0$, being the transition function, which is defined by its limits:

$$\nu(y) \rightarrow 1 \text{ for } y \gg 1 \text{ and } \nu(y) \rightarrow y^{-1/2} \text{ for } y \ll 1. \tag{3}$$

is derived from an action and obeys the standard conservation laws, with the generalised Poisson equation,

$$\triangle\Phi(\mathbf{x}) = 4\pi G\rho_{\rm b}(\mathbf{x}) + \nabla\cdot[\tilde{\nu}(|\nabla\phi|/a_0)\nabla\phi(\mathbf{x})], \tag{4}$$

$$\triangle\Phi(\mathbf{x}) = 4\pi G(\rho_{\rm b}(\mathbf{x}) + \rho_{\rm ph}(\mathbf{x})). \tag{5}$$

Here $\rho_{\rm b}(\mathbf{x})$ is the baryonic density, $\phi(\mathbf{x})$ the Newtonian potential, which fulfills the standard Poisson equation $\triangle\phi(\mathbf{x}) = 4\pi G\rho_{\rm b}(\mathbf{x})$, $\Phi(\mathbf{x})$ is the total gravitational potential and $\tilde{\nu}$ is the transition function between the Newtonian and the MOND regime, which is ν from Eq. 2 minus 1 with the limits: $\tilde{\nu}(y) \rightarrow 0$ if $y \gg 1$ (Newtonian regime) and $\tilde{\nu}(y) \rightarrow y^{-1/2}$ if $y \ll 1$ (MOND regime) with $y = g_N/a_0$. Several functions that fulfill this criterion have been used in the literature (see Lüghausen et al. 2015), but here

$$\tilde{\nu}(y) = -\frac{1}{2} + \frac{1}{2}\sqrt{1+\frac{4}{y}} \tag{6}$$

is used.[2]

Note that the second term on the right hand side of Eq.4 was condensed into

$$\rho_{\rm ph}(\mathbf{x}) = \frac{\nabla\cdot[\tilde{\nu}(|\nabla\phi|/a_0)\nabla\phi(\mathbf{x})]}{4\pi G}, \tag{7}$$

so the generalised Poisson equation also visualizes its quasi-linearity. Eq.5 shows that the total gravitational potential in MOND depends on the baryonic density

Начальные условия:

- Изолированное газовое облако,
- Сферической формы,
- С постоянной по объему плотностью газа,
- С твердотельным начальным вращением.
- Feedback можно задавать, а можно не задавать.

Face-on

Edge-on

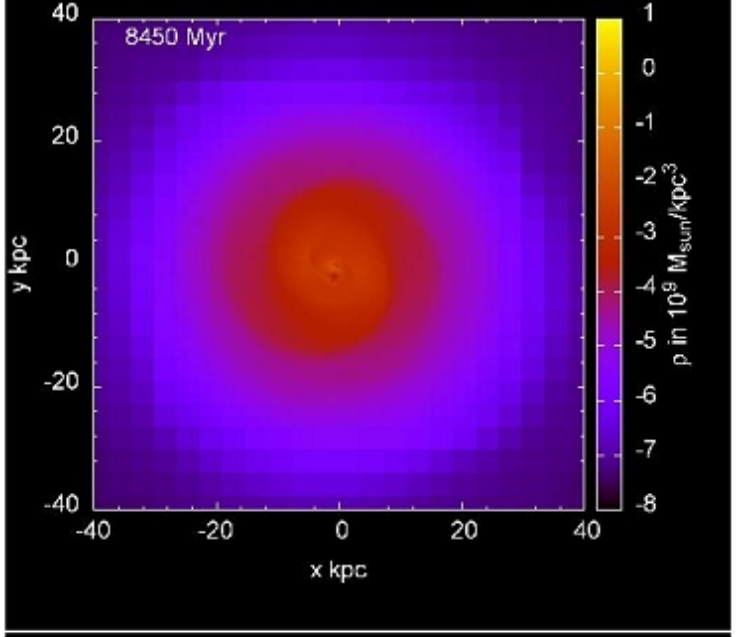

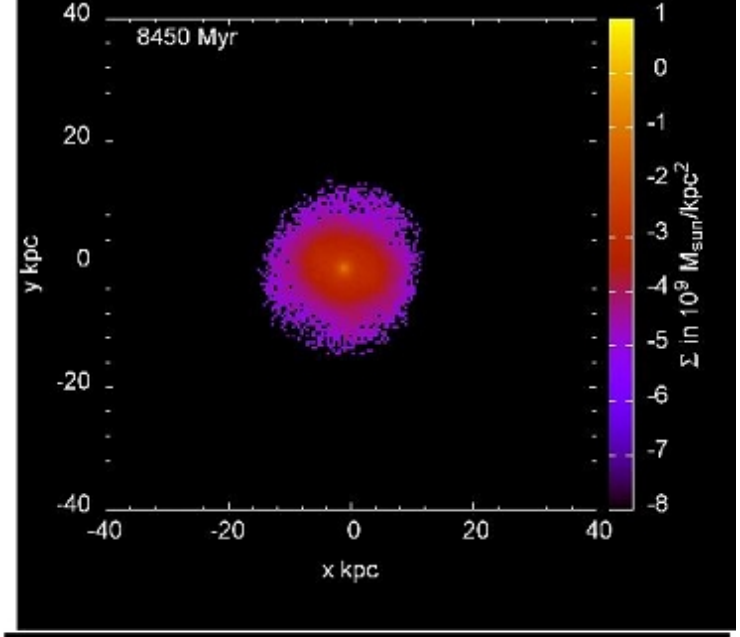

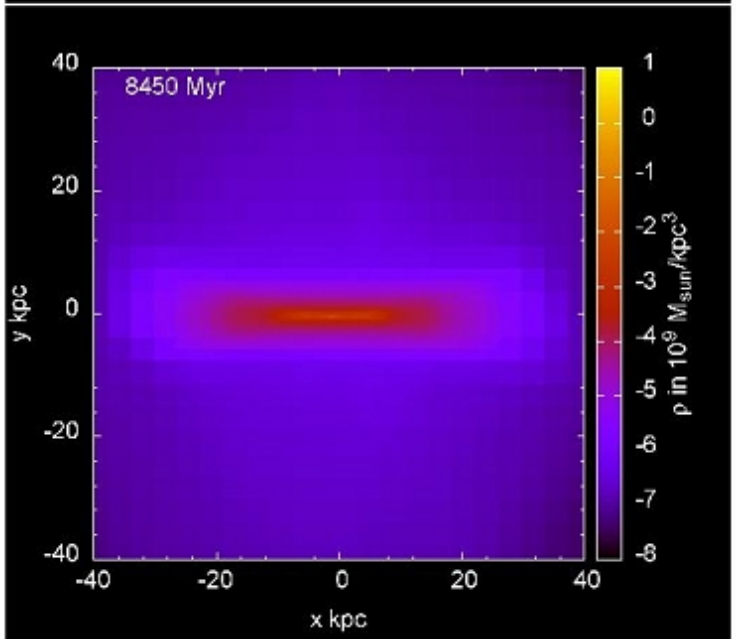

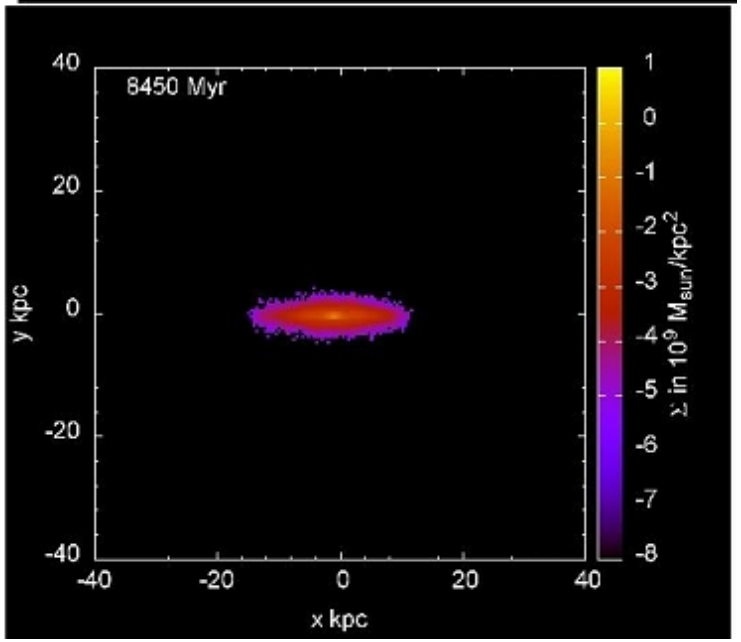

Gas

Stars

Плоская кривая вращения

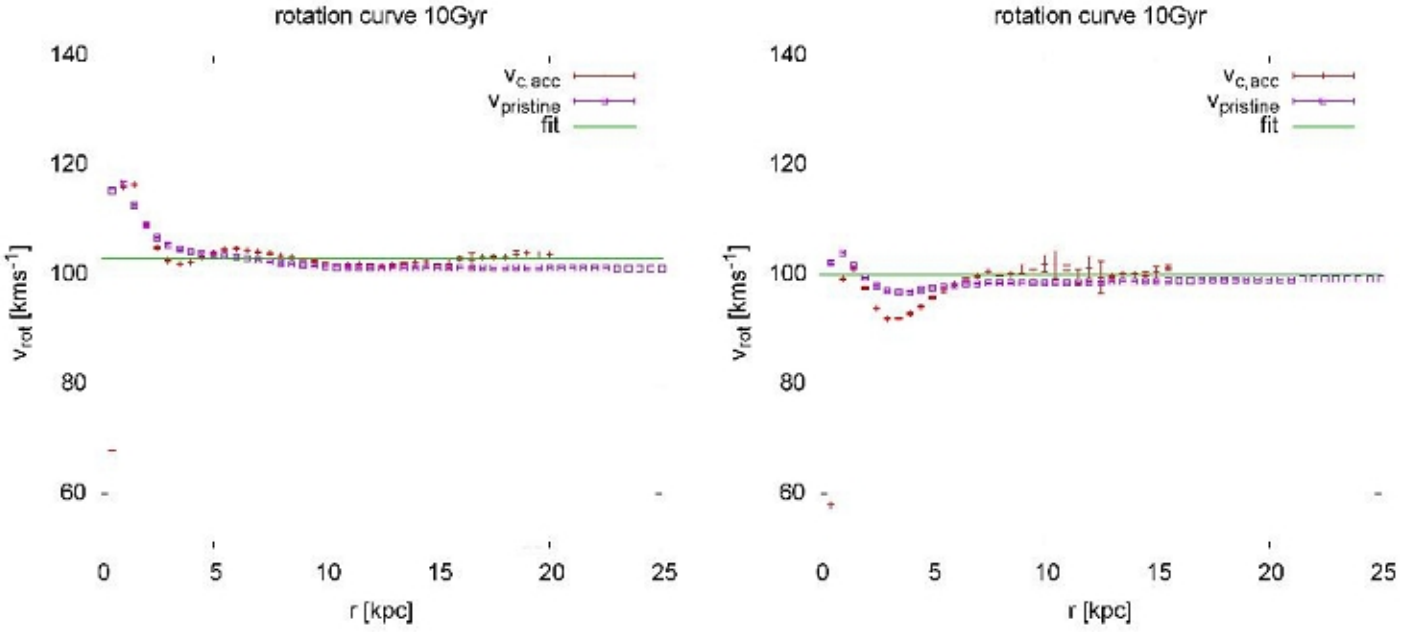

Figure 2. Rotation curves of both models with $r_{\rm init}$ = 20kpc shown in red, $v_{\rm c,acc}$, and the 'pristine' rotation curve of the respective model in purple. $v_{\rm c,acc}$ shows the rotation velocity calculated from the mean radial acceleration in the respective radial bin.*Left panel*: M1, *Right panel*: M1sn. See text for further detail on the computation and analysis.

+SN+RT

Экспоненциальные диски!

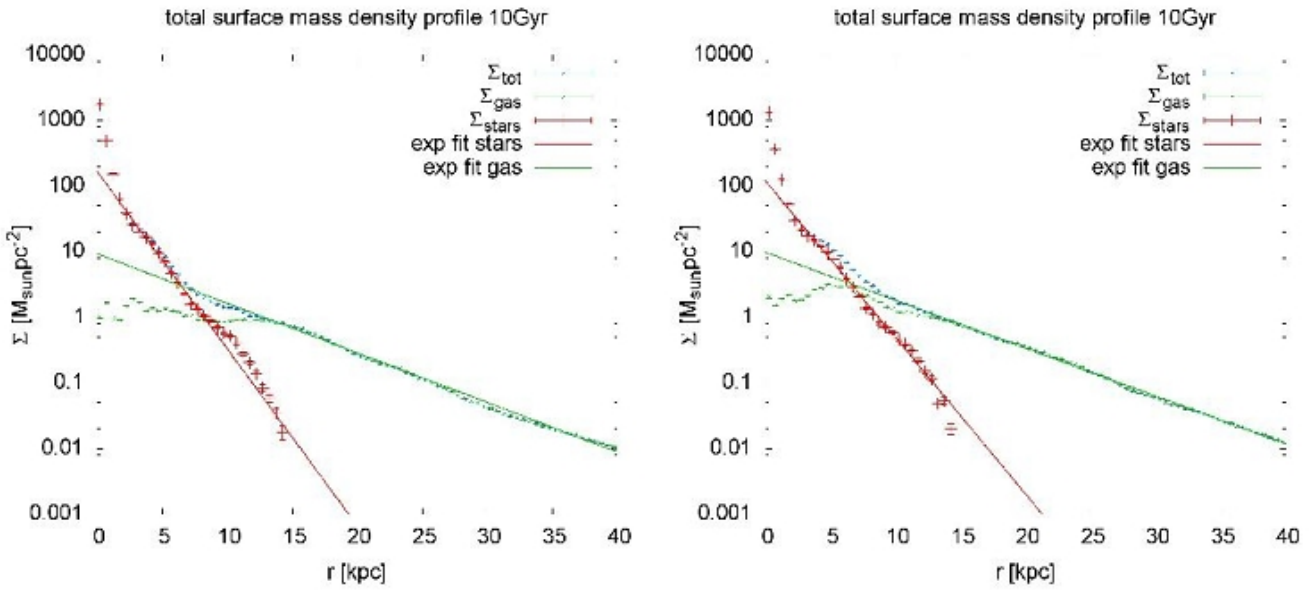

Figure 3. Surface mass density profiles of both models with $r_{\rm init} = 20$kpc. *Left panel*: M1, *Right panel*: M1sn. The red points correspond to the stellar surface mass density, the green ones to the surface mass density distribution of the gas and the blue ones show the total baryonic surface mass density distribution. The lines show the respective exponential fit to data.

Table 2. exponential scale lengths of M1, M1const, M2 and M3 for the stellar and gaseous surface mass distributions.

Model name	$r_{\rm e,stars}$[kpc]	$r_{\rm e,gas}$[kpc]
M1	1.61 ± 0.04	5.75 ± 0.06
M1const	1.19 ± 0.01	6.44 ± 0.07
M2	1.35 ± 0.01	7.24 ± 0.16
M3	1.98 ± 0.02	7.79 ± 0.10

Верхний предел по массе

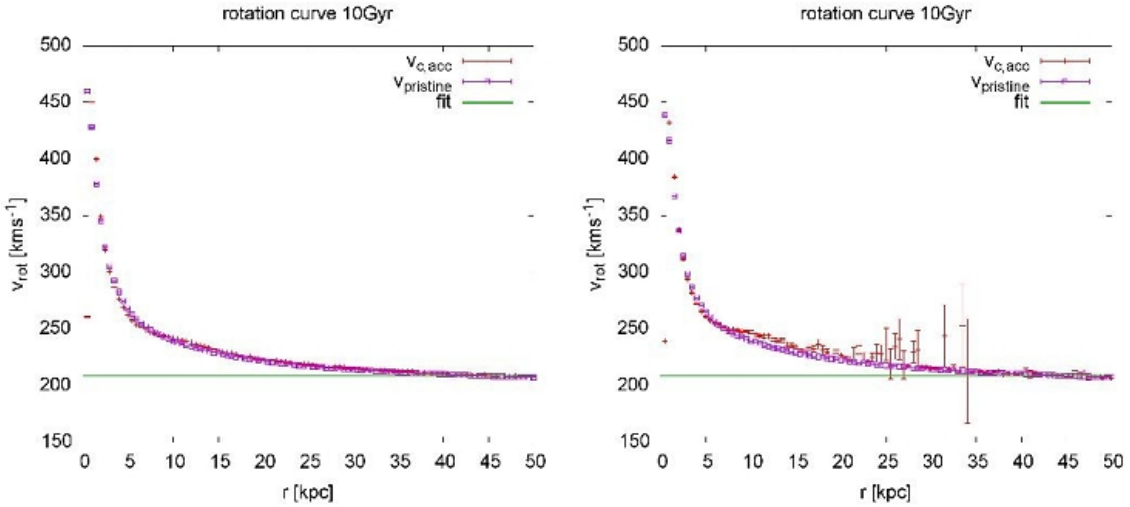

Figure 8. Rotation curves of both models with $r_{\rm init} = 50$kpc. *Left panel*: M4, *Right panel*: M4sn. See text for further detail.

Масса 10E11 масс Солнца

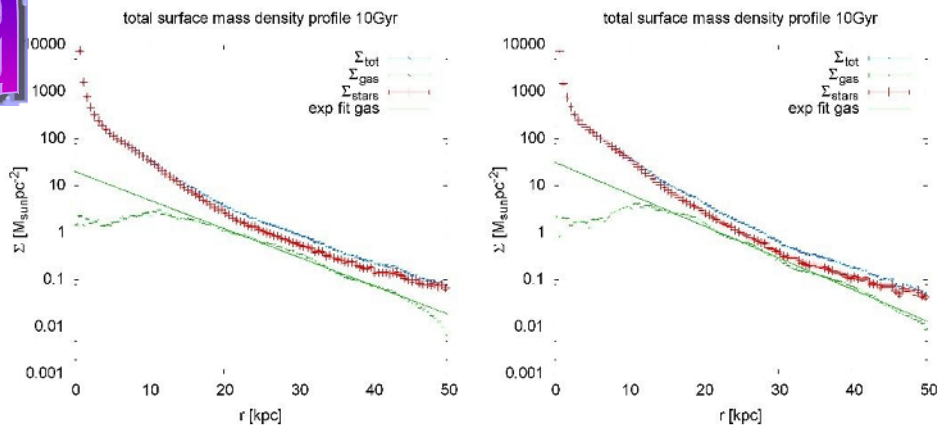

Figure 9. Stellar surface mass density profiles of both models with $r_{\rm init} = 50$kpc. *Left panel*: M4, *Right panel*: M4sn. The stellar surface mass density distribution does not follow a single exponential profile as the formation of these models is dominated by mergers of smaller satellites during and shortly after the initial collapse. The surface density profile may be approximated by more than one exponential profile (not attempted here though). See text for further detail.

Без аккреции: двойная экспонента в истории звездообразования

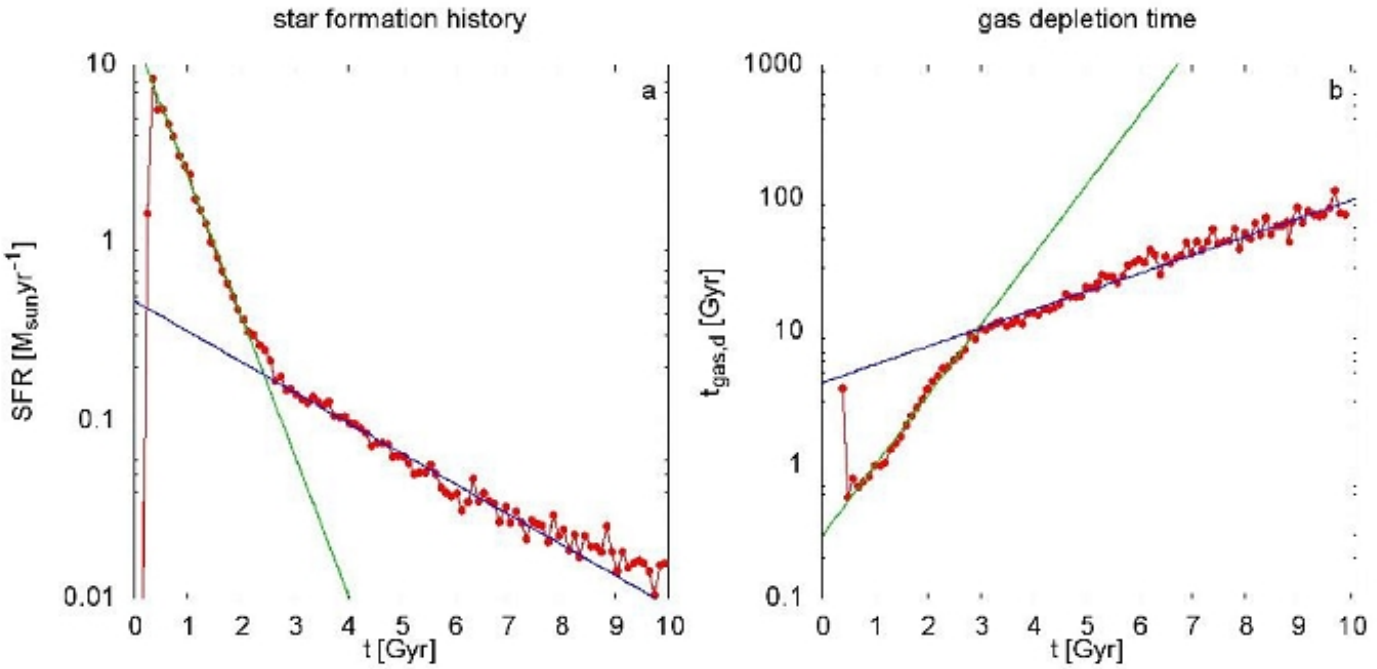

Figure 11. The star formation history (SFH) and the evolution of the gas-depletion time for M1. The red dots show the model data, the green line shows the exponential fit for the first part of the decaying star formation rate (SFR) / increasing gas-depletion time directly after the initial collapse. The blue line shows the exponential fit for the shallower part after most of the gas was converted into stellar particles during and shortly after the collapse.

Кенникат-Шмидт выполняется, главная последовательность – только вначале

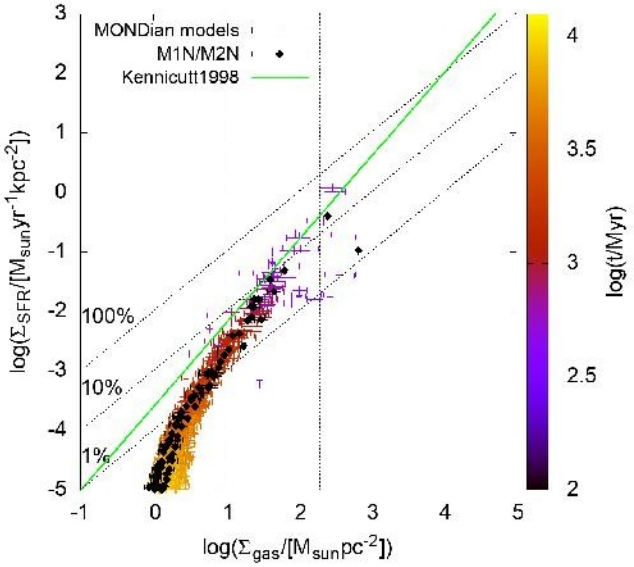

Figure 13. The KS-diagram for all 15 models shown as a time-evolution, while the age is indicated by colour. The Newtonian models are emphasized as black diamonds, though they show the same trend as all other models. The green line corresponds to the best fit to observational data by Kennicutt (1998), while the vertical dotted lines correspond

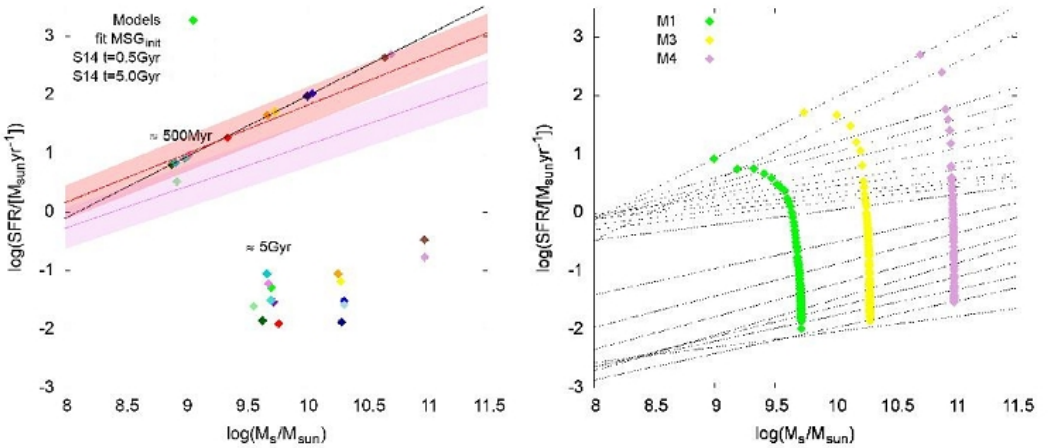

Figure 14. *Left panel*: The SFR-M_s plane with all models at their respective peak-SFR at the top and the distribution of the models 5Gyr afterwards at the bottom. The black line shows the linear fit to the peak-SFR data, resulting in $a = 3.66 \pm 0.35 \times 10^{-9} M_\odot yr^{-1}$ and $b = 1.041 \pm 0.004$. The colours are identical to Fig. 10 with the addition of M4=plum, M4sn=dark-plum and the Newtonian models indicated by light colours (e.g. M2=blue and M2N=light-blue). The red and violet areas show the observed main sequence of galaxies of Speagle et al. (2014) at $t = 0.5$Gyr and $t = 5.0$Gyr, respectively (Eq. 20). *Right panel*: The evolution of the linear fit to all models shown as the dashed lines at various times (see text) and the complete time-evolution of M1 (green), M3 (yellow) and M4 (plum).

Что еще хорошо:

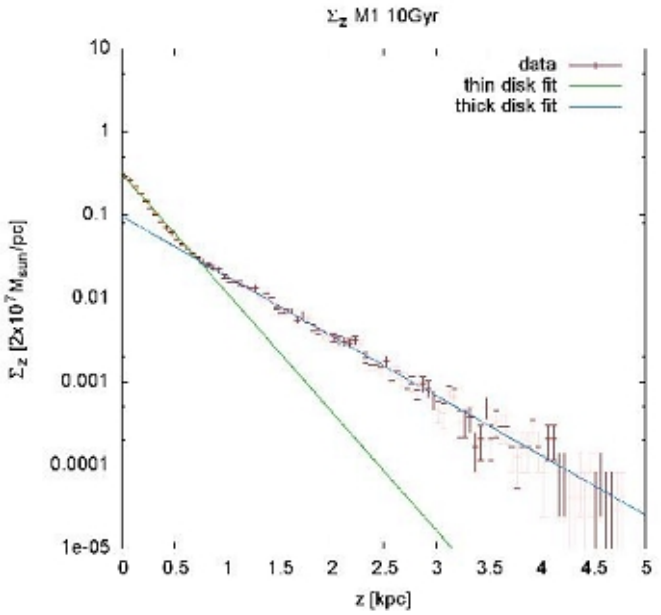

Figure 16. Mass distribution along the rotation axis (z-axis), Σ_z. The green line corresponds to the exponential fit for the thin disk and the blue line to the thick disk, fitted in the range $0 - 1$kpc and $1 - 3$kpc respectively (see text for details).

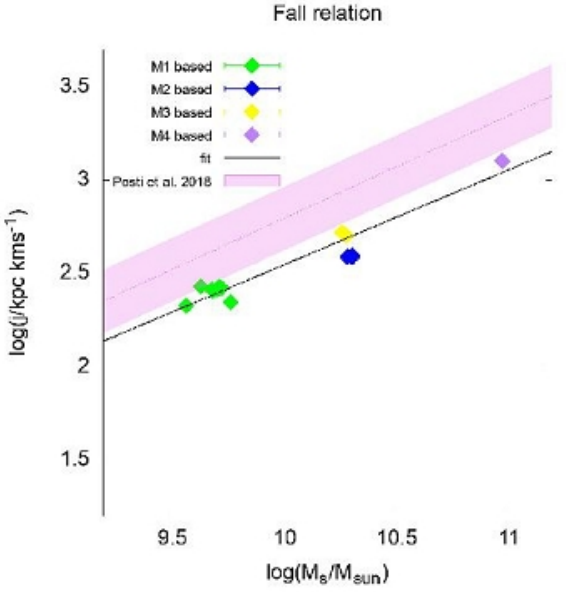

Figure 17. Relation between the specific stellar angular momentum, j_{star}, of all models with their respective stellar mass, M_{star} (Fall relation, computed here as for observations). The magenta area with the dashed line shows the observed data from Posti et al. (2018), the symbols for the different models are shown in the legend and the black line (Eq. 24) shows the best fit to the models. See text for further detail.

Наклон закона Фолла - правильный

Толстый диск - сам собой

Зато с RAR и барионным Талли-Фишером – никаких проблем

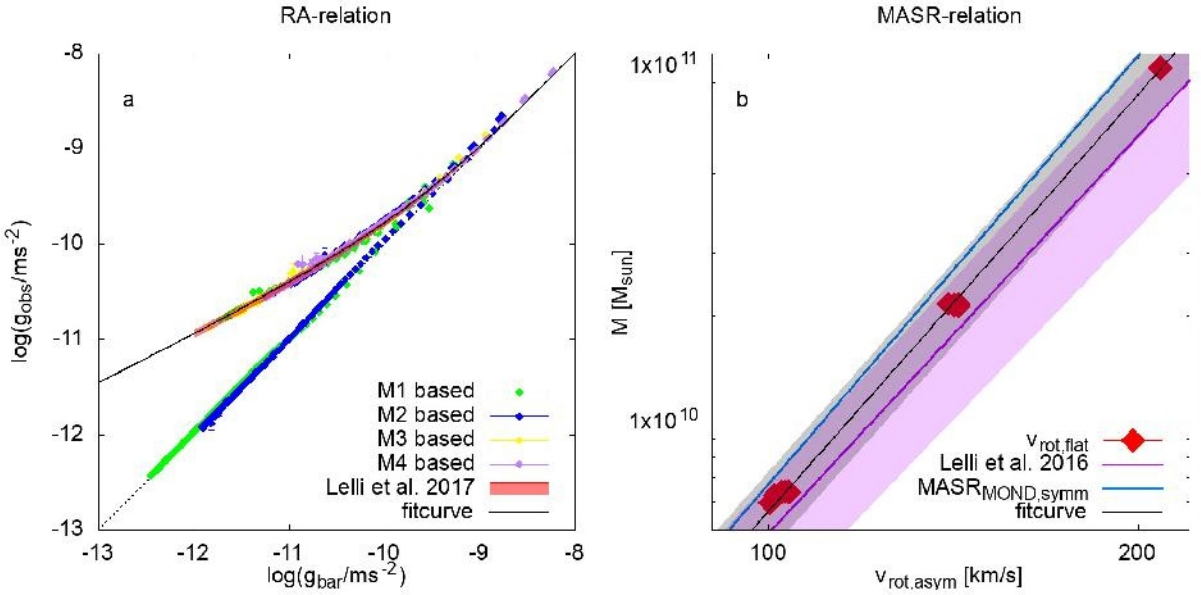

Figure 19. Comparison of the simulations with observed galaxy-scaling relations. Panel a shows the radial-acceleration relation of the data obtained directly from the accelerations in the simulations and the observational data from Lelli et al. (2017) (red area), the best fit to the data from all models (black solid line) and the purely Newtonian line, where $g_{\rm obs} = g_{\rm bar}$ (black dotted line). The colours of the models are shown in the legend. Panel b shows the MASR (BTFR) of the models (red diamonds), the best fit (black solid line) with uncertainties (grey area), the MASR (BTFR) in MOND assuming spherical symmetry (blue line) and the observational data from Lelli et al. (2016a) (magenta area).

ArXiv: 2002.01956

Constraining the Mass of the Emerging Galaxy Cluster SpARCS1049+56 at $z = 1.71$ with Infrared Weak Lensing

Kyle Finner,[1] M. James Jee,[1,2] Tracy Webb,[3] Gillian Wilson,[4] Saul Perlmutter,[5] Adam Muzzin,[6] and Julie Hlavacek-Larrondo[7]

[1] *Department of Astronomy, Yonsei University, 50 Yonsei-ro, Seoul 03722, Korea*
[2] *Department of Physics, University of California, Davis, One Shields Avenue, Davis, CA 95616, USA*
[3] *Department of Physics, McGill University, 3600 rue University, Montreal, Quebec, H3P 1T3, Canada*
[4] *Department of Physics and Astronomy, University of California Riverside, 900 University Avenue, Riverside, CA 92521, USA*
[5] *Physics Division, Lawrence Berkeley National Laboratory, 1 Cyclotron Road, Berkeley, CA, 94720, USA*
[6] *Department of Physics and Astronomy, York University, 4700 Keele St., Toronto, Ontario,MJ3 1P3, Canada*
[7] *Department of Physics, Universite de Montreal, Montrea, Quebec H3T 1J4, Canada*

Третье в этом проекте;
до этого на z=1.48 и 1.75, и все массивнее 10E14

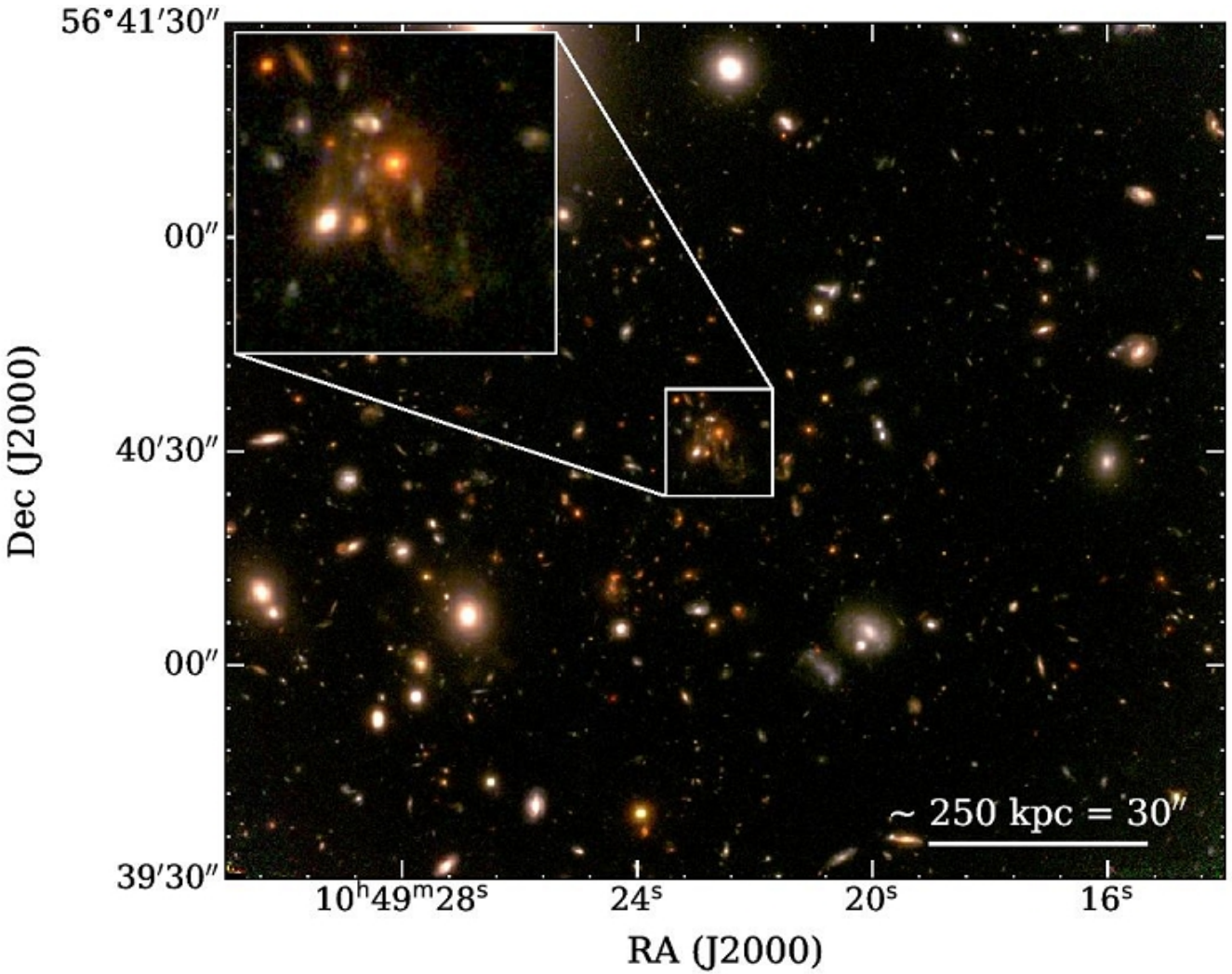

Figure 1. *HST* color-composite image of SpARCS1049 from stacking the F160W, F105W, and F814W filter images as RGB, respectively. The deep orange galaxy at the center of the image is the BCG ($10^h49^m22^s.6$, $56°40'33''$) and is shown in the inset image. The magnificent tidal feature discussed in Webb et al. (2015) is seen in the inset image stretching from the center to the southwest.

channel. This pipeline has been described in detail in

dense stellar fields that we tested for our PSF model-

Слабое грав. линзирование: восстановлена плотность по радиусу

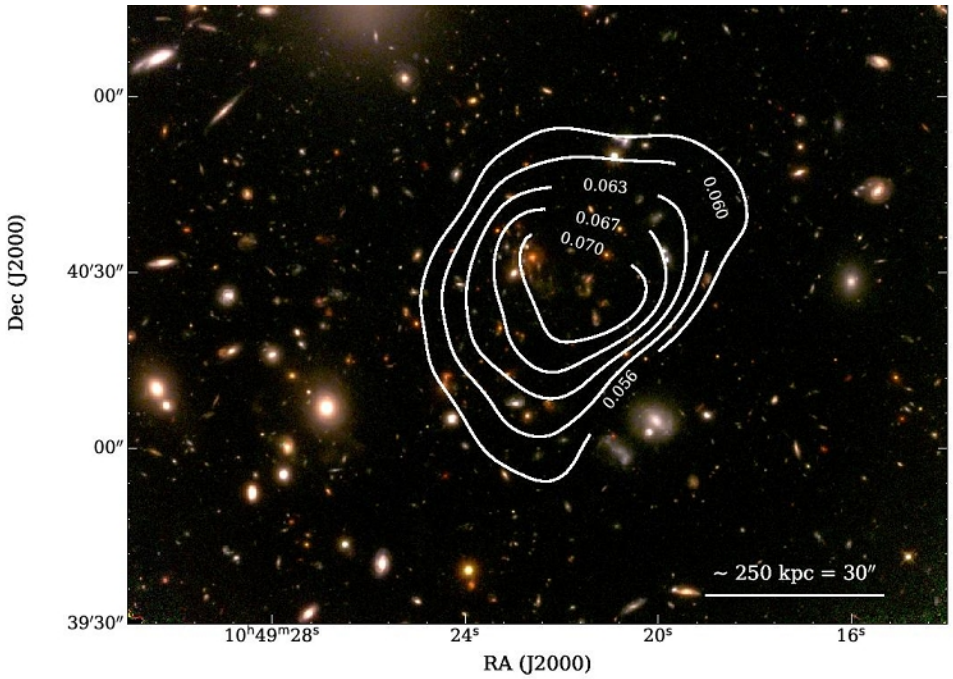

Figure 5. Mass reconstruction for SpARCS1049. Contour labels are subject to mass-sheet degeneracy. The distribution appears relaxed and does not show signs of substructures but does have a slight elongation in the east-west direction. The apparent offset of the mass peak and the BCG is shown to be insignificant through a bootstrap analysis. The significance (S/N) of the contours from the bootstrap result range from 2.0σ for the lowest contour to 2.5σ for the highest. The peak significance is 3.3σ.

Table 2. NFW density model fits to the tangential shear.

Model	c_{200}	M_{200c} $[\times 10^{14} \mathrm{M}_\odot]$	χ^2_r
Duffy et al. (2008)	2.2 ± 0.2	5.9 ± 3.5	1.27
Dutton & Macciò (2014)	3.1 ± 0.1	4.5 ± 2.3	1.16
Diemer & Joyce (2019)	4.5 ± 0.3	3.5 ± 1.2	1.03

Оценка интегральной массы – в 5 раз больше динамической

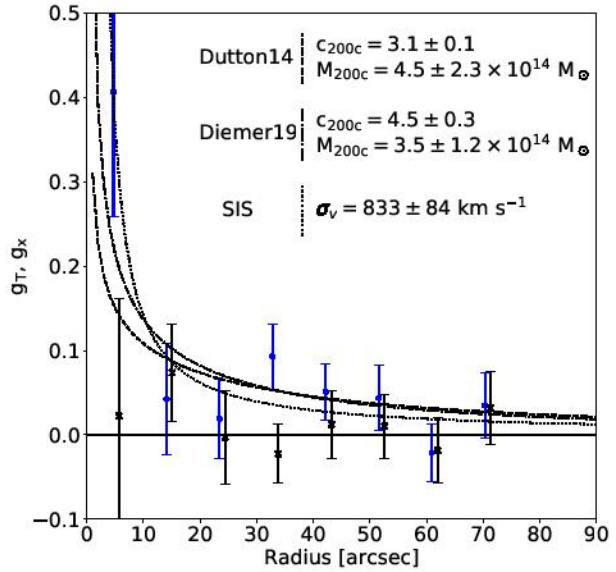

Figure 6. Density model fits to the tangential shear profile centered at the BCG. Blue circles are the tangential shear and black crosses are the cross shear. Error bars are the Poisson error. The cross shear has been shifted by 1″ for display purposes. Three density profiles are shown: the SIS sphere, the c-M relation of Dutton & Macciò (2014), and the c-M relation of Diemer & Joyce (2019).

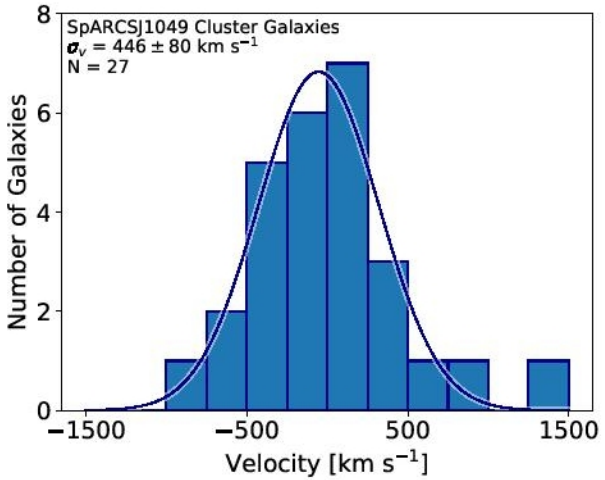

Figure 7. Velocity histogram of cluster member galaxies selected within 1500 km s^{-1} of the average velocity. The blue line is the best-fit Gaussian model. An Anderson-darling test fails to reject the null hypothesis that the galaxies follow a normal distribution.

Our WL mass estimate $M_{200} = 3.5 \pm 1.2 \times 10^{14}\ M_\odot$ provides the first mass estimate free of a dynamical equilibrium assumption. This mass estimate is consistent

Могут ли существовать такие массивные скопления на z~2?

We determine the rarity of this cluster by integrating the number of clusters above a minimum mass and redshift as

$$N(M,z) = \int_{z_{\rm min}}^{\infty} \int_{M_{\rm min}}^{\infty} \frac{dV(z)}{dz} \frac{dn}{dM} dM dz \qquad (8)$$

where dV/dz is the volume element and dn/dM is the mass function. We set the lower limits of the integrals to $z_{\rm min} = 1.71$ and $M_{\rm min} = 3.5 \times 10^{14}$ $M_{\odot}$, the central mass estimate. The exact upper limits of the integral are insignificant because the rarity of the cluster (steepness of the mass function in this regime) causes the integral to converge quickly. Using HMFCalc (Murray et al. 2013a), we adopt the mass function of Tinker et al. (2008) that has been updated by Behroozi et al. (2013). The estimated abundance of a cluster with mass and redshift of SpARCS1049 is ~12 over the full sky or ~0.01 clusters within the ~41.9 deg^2 footprint of SpARCS. Alter-

Пока статистика позволяет